Multi-tracer small animal PET imaging of the tumour response to the novel pan-Erb-B inhibitor CI-1033

Donna S. Dorow[1, 3], Carleen Cullinane[2, 3], Nelly Conus[3], Peter Roselt[1], David Binns[1], Timothy J. McCarthy[5], Grant A. McArthur[3, 4], Rodney J. Hicks[1, 4]

[1] Centre for Molecular Imaging, Peter MacCallum Cancer Centre, Melbourne, Victoria, Australia
[2] Pharmacology and Developmental Therapeutics Laboratory, Trescowthick Research Laboratories, Peter MacCallum Cancer Centre Melbourne, Victoria, Australia
[3] Translational Research Laboratory, Trescowthick Research Laboratories, Peter MacCallum Cancer Centre, Melbourne, Victoria, Australia
[4] Melbourne University Department of Medicine, St. Vincent's Hospital, Melbourne, Victoria, Australia
[5] Global Clinical Platforms, Pfizer Global Clinical Technology, Groton, Connecticut, USA

Received: 13 July 2005 / Accepted: 10 November 2005 / Published online: 1 February 2006

Abstract. *Purpose:* This study was designed as "proof of concept" for a drug development model utilising multi-tracer serial small animal PET imaging to characterise tumour responses to molecularly targeted therapy.
Methods: Mice bearing subcutaneous A431 human squamous carcinoma xenografts (n=6–8) were treated with the pan-Erb-B inhibitor CI-1033 or vehicle and imaged serially (days 0, 3 and 6 or 7) with [^{18}F]fluorodeoxyglucose, [^{18}F]fluoro-L-thymidine, [^{18}F]fluoro-azoazomycinarabinoside or [^{18}F]fluoromisonidazole. Separate cohorts (n=3) were treated identically and tumours were assessed ex vivo for markers of glucose metabolism, proliferation and hypoxia.
Results: During the study period, mean uptake of all PET tracers generally increased for control tumours compared to baseline. In contrast, tracer uptake into CI-1033-treated tumours decreased by 20–60% during treatment. Expression of the glucose transporter Glut-1 and cell cycle markers was unchanged or increased in control tumours and generally decreased with CI-1033 treatment, compared to baseline. Thymidine kinase activity was reduced in all tumours compared to baseline at day 3 but was sevenfold higher in control versus CI-1033-treated tumours by day 6 of treatment. Uptake of the hypoxia marker pimonidazole was stable in control tumours but was severely reduced following 7 days of CI-1033 treatment.
Conclusion: CI-1033 treatment significantly affects tumour metabolism, proliferation and hypoxia as determined by PET. The PET findings correlated well with ex vivo biomarkers for each of the cellular processes studied. These results confirm the utility of small animal PET for evaluation of the effectiveness of molecularly targeted therapies and simultaneously definition of specific cellular processes involved in the therapeutic response.

Keywords: Molecular imaging – Small animal PET – Tumour biology – FDG PET – Hypoxia

Eur J Nucl Med Mol Imaging (2006) 33:441–452
DOI 10.1007/s00259-005-0039-5

The first two authors contributed equally to the results presented in this report.

Rodney J. Hicks (✉)
Centre for Molecular Imaging,
Peter MacCallum Cancer Centre,
Locked Bag #1 A'Beckett Street,
8006 Melbourne, Victoria, Australia
e-mail: rod.hicks@petermac.org
Tel.: +61-3-9656-1854, Fax: +61-3-9656-1826

Introduction

Recent advances in the understanding of signalling pathways that regulate the growth of tumour cells have dramatically increased interest in the development of molecularly targeted anti-cancer therapeutics [1, 2]. As the results of large-scale cancer genomic and proteomic screens become available, the list of potential targets for such therapeutics is expanding rapidly. However, owing to the complicated nature of cellular networks that may be affected by a given treatment, and the high cost of bringing new drugs to the clinic, it is important to define the actual biological effects of targeted therapies early in the drug development process. While cell culture systems can be used to determine some therapeutic parameters, definition of functional effects in vivo is vital to predict the outcome of a novel treatment. For this reason, animal models of human cancers are important tools to aid development of molecularly targeted drugs. Among technologies that can be applied to preclinical studies of novel therapies, positron emission tomography (PET) is unique in combining the ability to image functional processes in vivo with high sensitivity and resolution, non-invasiveness and speed of data acquisition [3].

These properties are particularly relevant to imaging functional changes within tumours, and PET has become a valuable adjunct to diagnosis and monitoring of a range of human cancers [4–6]. Recent adaptation of PET for use with small animals has created a valuable opportunity for in vivo characterisation of new anti-cancer therapies in a cost-effective and timely manner [7–9].

Currently, the most prominent use of PET in cancer diagnosis and research involves visualisation of increased glucose metabolism in tumour cells with the glucose analogue [^{18}F]fluorodeoxyglucose (FDG). A range of biological processes can contribute to enhanced FDG uptake in tumours and these may have varying consequences for treatment outcome. For instance, tumour-associated processes such as altered blood flow due to angiogenesis and/or loss of micro-vessel organisation can have significant metabolic effects [10, 11]. Further, tumour hypoxia has the ability to potentiate glucose metabolism through hypoxia inducible factor 1α (Hif-1α) initiation of glucose transporter (Glut1) and hexokinase expression [12, 13]. In addition, heightened proliferation due to oncogene activation requires energy and ribose substrates for DNA and RNA synthesis, necessitating increased consumption of glucose. Recently, PET tracers have been developed that offer particular utility to probe mechanisms related to therapeutic response, including 3-deoxy-3-[^{18}F]fluorothymidine (FLT) to image cellular proliferation [14, 15] and ^{18}F-azoazomycin arabinoside (FAZA) [16, 17] to visualise tumour hypoxia. FLT is a fluorinated analogue of thymidine that is taken up by growing cells and phosphorylated by thymidine kinase 1 (TK1), trapping it within the cell [18, 19]. As TK1 activity increases in S phase and remains high through mitosis [20, 21], FLT retention is a marker for cell cycle phases other than G_0/G_1. FAZA is a fluorinated nitroimidazole retained within cells at a rate that is inversely proportional to the intracellular oxygen concentration [22]. Compared to the more established PET hypoxia tracer, fluoromisonidazole (F-MISO), FAZA has been suggested to have superior pharmacokinetic properties for high-definition imaging of tumour hypoxia [17]. Hypoxia is associated with poor prognosis in a variety of tumour types [23] and has been implicated as a major factor in resistance of tumours to both radiation and chemotherapy. The ability to image processes associated with tumour proliferation and hypoxia in vivo promises to provide much broader insights into molecular events accompanying responses to targeted therapies.

One group of molecules of particular interest as targets for anti-cancer therapy is the epidermal growth factor receptor (EGFR)/Erb-B family of cell surface tyrosine kinase receptors [24]. Deregulation and/or over-expression of EGFR/Erb-B family members occurs in a variety of tumour types, in some cases correlating with aggressiveness of tumour phenotype [25–27]. Recently, a number of small molecule inhibitors targeting EGFR/Erb-B kinase activity have been identified as anti-tumour agents [28]. A newer member of this class of therapeutic agents is the pan-Erb-B specific tyrosine kinase inhibitor CI-1033, currently in clinical development [29]. CI-1033 is a quinazoline-based irreversible inhibitor that acts by alkylating a cysteine in the kinase domain of Erb-B proteins, thereby blocking catalytic activity and downstream signalling [30, 31]. CI-1033 is effective in arresting growth of a number of in vitro tumour models and has shown particular promise in blocking tumour growth when used in combination with DNA-damaging agents or radiation [32, 33]. However, to date scant information is available about the effects of CI-1033 treatment on specific tumour processes in vivo.

Herein we report the results of a small animal imaging study in which FDG, FLT and FAZA PET have been used together with ex vivo biomarker studies to characterise molecular events during the tumour response to CI-1033. To our knowledge, this is the first study in which the three PET tracers have been employed to follow anti-tumour therapy in a single biological system. As well as offering insights into functional activities of CI-1033 in vivo, results of these studies highlight the effectiveness of small animal PET in defining molecular events associated with tumour responses to targeted therapies. The combination of PET with conventional molecular biological tools offers a paradigm for translational research focussed on evaluation of the emerging class of molecularly targeted anti-cancer therapeutics.

Materials and methods

Materials

PET tracers were synthesised and labelled in a dedicated in-house radiochemistry facility. ^{18}FDG was purchased from Cyclotek (Melbourne, Australia) and ^{18}F–MISO from the Austin Hospital PET Centre (Melbourne, Australia). ^{18}Fluoride was produced using an OSCAR 7 cyclotron (Oxford Instruments, Oxford, UK) by the ^{18}O(p,n)^{18}F nuclear reaction. ^{18}FLT was produced according to the method of Machulla et al. [34] and ^{18}FAZA according to the method of Piert et al. [35]. Final purity and radiochemical identity of tracers were assessed by high-performance liquid chromatography, following standard protocols. CI-1033 was obtained from Pfizer Australia, dissolved in H_2O at a concentration of 2 mg/ml and daily aliquots frozen at −20°C. Rabbit anti-human Glut1 antibody (DAKO Cat # A3536) was used a concentration of 10 μg/ml, rabbit α human Ki-67 (Ab4, Neomarkers Cat # RB 1510-P1) at 10 μg/ml, affinity purified rabbit anti-active human caspase 3 (R&D Systems Cat # AF835) at 0.2 μg/ml and anti-BrdU (B44, Becton Dickinson) at a dilution of 1:50. Hydroxyprobe-1 (MAB-1 anti-pimonidazole monoclonal antibody) was from NPI (Belmont, MA, USA).

Tumour growth, drug treatment and imaging

A431 human squamous cell carcinoma cells (ATCC) were cultured in alpha MEM supplemented with 10% FBS in 5% CO_2 in air at 37°C. Female Balb/c nude mice 8–11 weeks old were inoculated s.c. on the right hind limb (FDG and FLT studies) or above the right forearm (FAZA/F-MISO study) with 3×10^6 A431 cells in PBS. Tumours were measured twice weekly using electronic callipers and tumour volumes calculated using the formula [volume=length/2×width^2]. Once tumour volumes had reached approximately 150 mm^3, animals were randomised into test and control groups (day 0). For FDG PET, animals were fasted for 3 h, then anaesthetised by inhalation of 2.5% isoflurane/50% O_2 in air (flow rate 200 ml/min). Anaesthetised animals were injected via the lateral tail vein with 300–600 μCi (11–

22 MBq) ^{18}FDG in 100 µl saline and anaesthesia maintained for 20 min following tracer injection to minimise muscle activity during the initial uptake period. For FLT and FAZA PET studies, non-fasted animals were injected un-anaesthetised with ^{18}FLT, ^{18}FAZA or ^{18}F-MISO, as above.

For all scans, animals were anaesthetised as above approximately 1.5 h (FDG and FLT) or 3 h (FAZA) post tracer injection and scanned for 5–10 min on a prototype A-PET (Phillips Mosaic) small animal PET scanner [36]. Upon completion of PET scans on day 0, daily treatment with CI-1033 (20 mg/kg p.o.) was commenced [31]. Tumours were measured and PET scanning repeated as described above on days 3 and 6 or 7. PET images were reconstructed using the 3-D RAMLA algorithm [37, 38] and images displayed using standard image software available on the A-PET scanner. Tracer uptake was measured using region of interest (ROI) software on the A-PET workstation. Briefly, ROIs were manually placed around the tumour and an average background region on transaxial slice images displayed on the workstation. The background ROI was chosen to represent tracer present within the blood pool and non-tumour tissue, excluding regions of increased uptake such as heart or brown fat for FDG and visceral regions for FLT and FAZA. Maximum, minimum and average pixels within the ROI per slice were automatically stored as data files. Uptake ratios were then calculated by dividing the maximum value of pixels within a tumour ROI by the average value of pixels within the background ROI. The resolution of the A-PET scanner is 2.2 mm and the average tumour diameter for all groups of animals was greater than 4 mm on all imaging days; therefore correction for partial volume effect was not required.

Ex vivo analysis of retained radioactivity

Following the final PET scan on days 6 or 7, animals were sacrificed and blood, tumour and thigh muscle tissues removed, weighed and placed into flat bottom tubes. Disintegrations at 511 keV±15% were quantified in a well counter (187-950-A100 MCA, Biomedex Medical Systems) attached to a multichannel analyser interfaced with Atomlabs 950 software (Biomedex Medical Systems).

Ex vivo biomarker studies

Tumours were implanted, grown and treated as for the PET experiments. Each animal was injected with BrdU (100 mg/kg body weight) 1 h prior to sacrifice. Three baseline animals were sacrificed on day 0, and three each from the control and test groups were sacrificed on days 3 and 6. Immediately after sacrifice, half of each tumour was fixed in 4% buffered formalin for immunohistochemistry (IHC) and the remainder snap frozen in liquid nitrogen and stored at −70°C for protein extraction. To assess changes in tumour hypoxia, a separate cohort of A431 xenograft bearing mice were treated with either CI-1033 or vehicle as for the PET studies. These mice were sacrificed on day 7, 3 h after i.p. injection of 60 mg/kg pimonidazole, and tumour tissues were fixed as above for anti-pimonidazole IHC.

Immunohistochemistry

Fixed tissues were embedded, cut into 3-µm sections, de-waxed and probed with antibodies following standard procedures. For Ki-67, active-caspase 3 and Glut1 IHC, antigens were retrieved in 10 m*M* sodium citrate buffer, pH 6.0, for 2 min in a pressure cooker. Slides were loaded onto a DAKO Autostainer and all subsequent procedures carried out on the machine at room temperature. Endogenous peroxidase activity was quenched in 3% H_2O_2 (10 min) before incubation with rabbit primary antibody (30 min). Bound antibody was detected using the polymer linked detection system (EnVision+, DAKO) with DAB+ visualisation (DAKO). Sections were counterstained with haematoxylin and mounted in DPX.

For BrdU IHC, tissues were treated as above and the staining procedure completed manually as previously described [39]. Briefly, antigens were retrieved with pepsin and denatured with 2 *M* HCl and neutralised in 0.1 *M* borate buffer, pH 8.5. Endogenous peroxidase activity was quenched in 10% methanol, 3% H_2O_2 in PBS before probing with anti-BrdU antibodies (60 min at room temperature). Bound antibody was detected using the LSAB-2 detection system (DAKO) with DAB conversion, then sections were counterstained and mounted as above. Pimonidazole IHC was performed using DAKO ARK mouse antibody detection kit following the manufacturer's directions.

Scoring of IHC

Stained tissue sections were examined on a Zeiss Axioskop 2 light microscope equipped with a computer networked digital camera. For each tumour section, six high-power (400×) fields were photographed and the resulting Tiff images printed on a colour printer with a superimposed counting grid. Cells were scored from the printed images as either positively stained (irrespective of staining intensity) or unstained. A total of 18 high-power images (six fields per section, three tumours per group) were scored for each group per time point. The percentage of positively stained cells in the six images per tumour was calculated and a mean percentage (n=3) for each group graphed, with error bars representing standard deviation from the mean. Significance values were calculated using the unpaired t test.

TK1 activity assay

Thymidine kinase activity was assayed as described by Stuart et al. [40] with minor modifications. Briefly, snap-frozen tissue was powdered on dry ice, homogenised in 50 mM Tris-HCl pH 7.5, 3.6 m*M* β-mercaptoethanol and 0.5% Nonidet P-40 and incubated for 30 min on ice. Lysates were cleared by centrifugation (3×5 min at 12,000 *g*), protein concentration determined by Dc Protein Assay Kit (Bio-Rad) and aliquots frozen in liquid nitrogen for storage at −70°C. For assay, thawed extracts (80–100 µg protein) were adjusted to 40 µl of extraction buffer containing 15 m*M* NaF, 5 m*M* ATP, 2.5 m*M* $MgCl_2$, 0.08 m*M* unlabelled thymidine and 50 µCi ^{3}H-thymidine (23 µCi/mmol). Reactions were allowed to proceed for 20 min at 37°C, stopped in boiling water (2 min) and cleared by centrifugation (5 min at 12,000 *g*). Aliquots of the cleared reaction mix (20 µl) were spotted onto Whatman DE81 anion-exchange paper discs in duplicate and the discs washed in 1 m*M* ammonium formate (2×5 min) and then 1× in MeOH before drying. Deoxythymidine monophosphate (dTMP) was eluted from the disks into 1 ml of 0.1 *M* HCl, 0.2 *M* KCl with shaking for 30 min. Liquid scintillant (5 ml) was added and the vials shaken for 5 h or overnight before counting. Results are expressed in pmol deoxythymidine converted to dTMP per minute per mg protein.

Results

The A431 human squamous cell carcinoma cell line overexpresses EGFR and has thus been used extensively to demonstrate the effectiveness of Erb-B family targeted anti-cancer therapeutics [31, 41, 42]. In the present study, multi-tracer serial PET imaging was employed to follow

biological responses of A431 tumour xenografts to treatment of mice with CI-1033. Using conventional tumour volume measurements, CI-1033 was shown to be highly efficacious against the A431 tumour model, with tumour regression evident by day 3 (Table 1). Tumour volumes averaged approximately 150 mm^3 at day 0 of each imaging study and in CI-1033-treated animals the average tumour volume was 50–100 mm^3 by the final imaging day. In contrast, volumes of control tumours increased over the treatment period, averaging 300–400 mm^3 at day 6/7.

For PET imaging experiments, tumour uptake of each tracer was determined from PET images by calculating the ratio of the maximum pixel value within a tumour ROI to the average pixel value within a background ROI representing the blood pool and non-tumour tissue (see Materials and methods section). While not an absolute measure of the tracer dose retained within the tumour, this quantification method has several advantages for the present study. Firstly, with the very small volumes required for lateral tail vein injections in mice (less than 200 μl), extravasation during injection can significantly affect the final dose of tracer that enters the bloodstream. Such losses are extremely difficult to eliminate in serial tail vein injections. Also, absolute quantification of uptake from PET images requires correction for signal attenuation, and software for this parameter was not available on the PET scanner used for this study. Furthermore, tumour to background ratios calculated by the described method are independent of tumour volume and therefore suitable for comparison of tracer uptake in treated and untreated tumours for a model in which tumour regression accompanies treatment (see Table 1). However, to confirm the validity of the quantification method, tumour to blood and tumour to muscle ratios were also calculated from ex vivo counting of retained tissue radioactivity following the FDG PET experiment.

Metabolic response of A431 tumours treated with CI-1033

The effect of CI-1033 on tumour metabolism as measured by uptake of FDG was compared with the effect on expression of the glucose transporter, Glut1 (Fig. 1). Mice were scanned with FDG PET on days 0, 3 and 7 and resulting images for typical control and CI-1033-treated mice are shown in Fig. 1a. As well as illustrating the relative decrease in FDG uptake in tumours of CI-1033-treated versus control animals during treatment, these images provide visual representation of the intensity of radioactive signal in tumour versus background regions of the scanned image. In general, the images show fairly homogeneous FDG uptake throughout the tumour mass; however, some reduction in signal toward the centre of larger tumours is often observed, consistent with the development of a central necrotic core. Typically, increased FDG uptake is also evident in tissues with high glucose utilisation, including heart muscle, brown fat of the upper back and the harderian glands near the eyes. As FDG is cleared through the urinary system, a signal of varying intensity is also visible in the bladder.

Tumour to background ratios calculated from FDG PET image ROI pixel values for all animals in the FDG arm of the study averaged 5.4 at baseline (day 0). Relative ratios for control and CI-1033-treated animals are presented in Table 2 as the mean percentage change at days 3 and 7 compared to baseline. These data reveal a significant difference in tumoural FDG uptake between control and CI-1033-treated animals on both scanning days. Interestingly, despite increased volumes of control tumours over the 7-day treatment period (Table 1), tumoural FDG uptake remained reasonably constant in this group over 7 days. In contrast, FDG uptake into tumours of CI-1033-treated animals was reduced to approximately 60% of baseline at day 3, thereafter falling to about 40% of baseline by day 7 ($p<0.001$, paired t test). As CI-1033 treatment caused a significant reduction in tumour volume over the treatment period (Table 1), the level of FDG uptake was confirmed by ex vivo counting of tumour, blood and muscle tissue following the final PET scan on day 7 (Fig. 1b). The ex vivo count data are expressed as ratios of radioactivity per gram of tumour tissue ($n=8$) to that of either blood (T:B) or muscle (T:M). FDG retention ratios determined by this method are consistent with uptake ratios calculated from PET scans showing reduced uptake per gram into tumours of CI-1033-treated animals compared to controls.

To validate metabolic effects of CI-1033 treatment, tumours were assayed for expression of the glucose transporter, Glut1 [43, 44] at time points coinciding with PET imaging. Examples of typical Glut1-stained tumour sections from day 3 control and CI-1033-treated mice are shown in Fig. 1c. In this study, most cells in baseline (not shown) and control sections had intense staining, most prominently associated with the cell membrane. In the CI-1033-treated sections at both day 3 and day 6 (not shown), the majority of cells displayed low intensity cytoplasmic staining, with only a few isolated cells retaining higher levels of Glut1 signal. Scoring of positive cells (Fig. 1c, graph) confirmed that greater than 95% of cells in untreated tumours expressed Glut1 throughout the study period while in CI-1033-treated tumours the percentages of positively stained cells dropped to 79% at day 3 ($p=0.0016$) and 75% at day 6 ($p=0.0020$), compared to baseline.

Table 1. Relative tumour volume ratios[a]

Group[b]	FDG		FLT		FAZA	
	Day 3	Day 7	Day 3	Day 6	Day 3	Day 6
Control	1.54	1.97	1.63	2.34	1.54	2.49
CI-1033[c]	0.71	0.26	0.79	0.47	0.74	0.33

[a]Mean increase or decrease in tumour volume relative to that on day 0
[b]FDG, $n=8$; FLT, $n=7$ for control, $n=8$ for CI-1033; FAZA, $n=6$
[c]CI-1033 20 mg/kg in H_2O vehicle, p.o. daily [32]

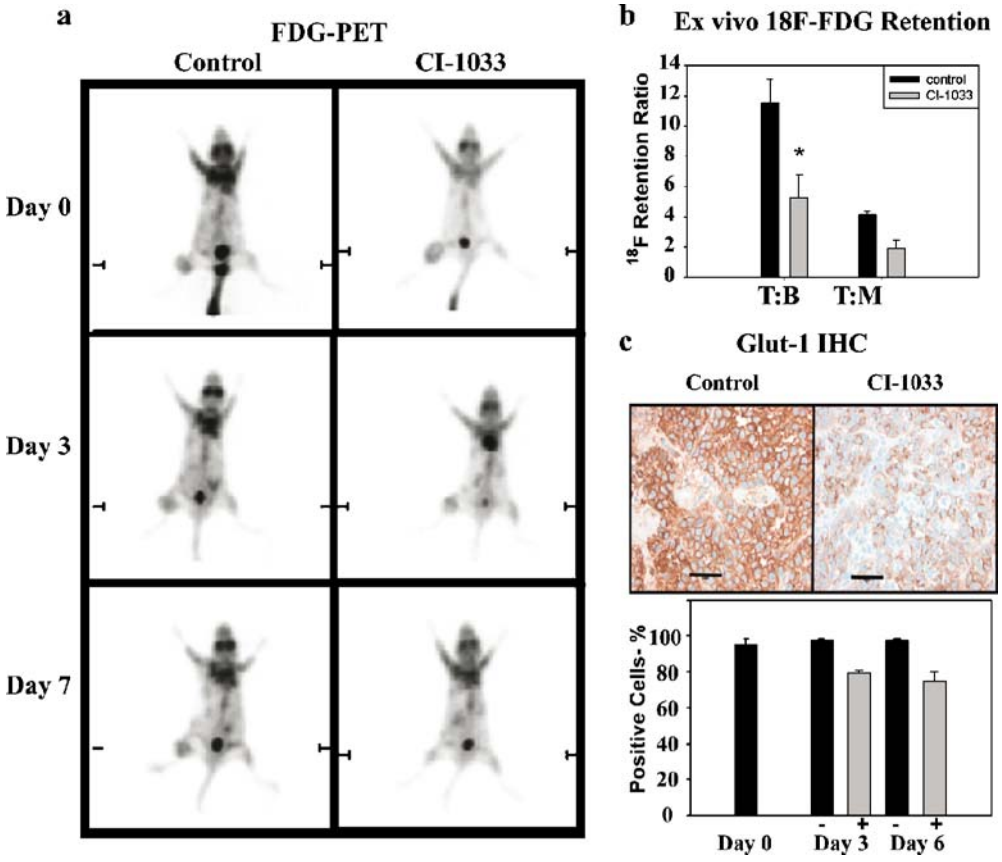

Fig. 1. FDG PET monitoring of CI-1033 treatment. **a** Examples of FDG PET images for typical control and CI-1033-treated animals shown as planar views, ventral side upwards. Mice were given 20 mg/kg CI-1033 or H_2O vehicle p.o. daily beginning on day 0 and were scanned with FDG PET on days 0, 3 and 7. **b** Ex vivo counting of retained radioactivity. Animals were sacrificed following the final PET scan and radioactivity at 511 keV quantified per gram of tumour, blood and muscle tissue. Ratio of counts in tumour to blood (*T:B*) or muscle (*T:M*) are presented as mean±SEM (n=8 per group). * Significant (P<0.05) reduction in uptake relative to that of the control group (unpaired t test). **c** Anti-Glut1 IHC. Examples of day 3 tumour sections from control (*left*) and CI-1033-treated (*right*) mice stained with anti-Glut1 antibodies. Animals (n=3) treated as for the PET study were sacrificed on days 0, 3 and 6, and tumours were excised and assayed by IHC with anti-Glut1 antibodies as described in the Materials and methods section. The graph shows mean percentages ±SD of Glut1-positive cells in control (*black bars*) and CI-1033-treated (*grey bars*) sections at days 0, 3 (P=0.0016) and 6 (P=0.0020; unpaired t test)

Effect of CI-1033 on tumour proliferation

To evaluate CI-1033-mediated alterations in processes associated with cellular proliferation, A431 tumour-bearing mice were imaged during treatment with the thymidine-based PET tracer, FLT (Fig 2). Typical FLT PET images for control and CI-1033-treated mice (Fig. 2a) revealed a little change in FLT uptake into tumours of control animals during the treatment period and a concomitant decrease in uptake into CI-1033-treated tumours.

Tumour to background ratios from FLT PET images for all animals averaged 8.4 at baseline. Mean uptake ratios

Table 2. Relative PET uptake ratios[a]

Group[b]	FDG		FLT		FAZA	
	Day 3	Day 7	Day 3	Day 6	Day 3	Day 6
Control	1.14±0.07	1.00±0.06	1.30±0.21	1.20±0.17	0.96±0.12	1.28±0.09
CI-1033	0.59±0.07	0.41±0.08	0.80±0.06	0.60±0.10	0.48±0.12	0.43±0.14
P value[c]	0.003	0.001	NS	NS	0.004	<0.001

[a]Mean change in tumour to background ratio ±SEM, compared to baseline (day 0)

[b]FDG, n=8; FLT, n=7 for control, n=8 for CI-1033; FAZA, n=6

[c]Significance value (t test) for CI-1033-treated vs control tumours; *NS* not significant

calculated from PET images for the two treatment groups (Table 2) confirmed that FLT uptake decreased during CI-1033 treatment. The relative reduction in FLT uptake into tumours of the CI-1033-treated group was approximately 20% compared to baseline at day 3 and 40% by day 6, both values being significant ($p<0.001$). While the tumours of control animals showed a time-dependent trend towards increased FLT uptake, differences in uptake between control and treated tumours were not significant on either imaging day (Table 2). This was most likely due to variability in FLT uptake among control tumours, where a significant amount of signal heterogeneity was observed in the quickly growing tumours of this group, particularly at day 3. Figure 2b shows an example of heterogeneity in FLT uptake that typified control tumours in the study, which is highlighted in images of transaxial, sagittal and coronal sections through the centre of the tumour region of the image.

As thymidine kinase (TK) activity is the major determinant of FLT retention in tumours [45], the effect of CI-1033 on tumour TK activity was assayed biochemically (Fig. 2c). CEM cells with tetracycline-inducible expression of the cell cycle inhibitor p16 were used as a positive control in this assay. Induction of p16 expression in these cells with doxycycline treatment induces G1 arrest and results in a large reduction in TK activity (Fig 2c, right panel). In the control tumour samples (left panel), TK activity was variable, being reduced at day 3 (7.25±1.9 pmol/min/mg protein) but increased at day 6 (22.9±2) relative to baseline (14.9±2.64). This is in keeping with the variability in FLT uptake observed in the PET study and may also be attributable to heterogeneity of uptake into the faster growing control tumours. In contrast, TK activity in CI-1033-treated tumours was reduced on both sampling days (day 3=8.2± 1.5, day 6=3.26±0.5), as compared with baseline. Thus after 6 days of CI-1033 treatment, TK activity was significantly reduced in CI-1033-treated tumours compared to baseline, consistent with the data for CI-1033-treated tumours in the PET study.

To further examine the relationship between FLT uptake and cell cycle-related changes in the CI-1033–A431 model, tumours were assayed by IHC for levels of Ki-67 expression and incorporation of BrdU. Examples of anti-Ki-67-stained sections for control and CI-1033-treated tumours at day 6 are shown in Fig. 2d. In control sections, a very high percentage of cells stained positively for Ki-67. In CI-1033-treated sections, staining was undetectable in a percentage of cells but many still retained some level of staining and a few of these were very highly stained. Overall, however, there was a clear reduction in intensity of Ki-67 staining in the CI-1033-treated tumour sections compared to controls (Fig. 2d, left panels). Quantification of positively stained cells disregarding staining intensity (right panel) showed that more than 90% of cells in control tumours expressed Ki-67 throughout the treatment period. By comparison, percentages of positively stained cells in the CI-1033-treated tumours decreased to 83% at day 3 and 65% at day 6.

In the BrdU incorporation assay, striking differences between control and CI-1033-treated tumours were noted on both post-treatment sampling days. These differences are clearly seen in the examples of day 3 anti-BrdU-stained tumour sections (Fig. 2e), where the numbers of positively stained nuclei are seen to be dramatically reduced in the CI-1033-treated tumour compared to the control section. Quantification of anti-BrdU-stained cells (right panel) revealed that the extent of BrdU incorporation in the control tumours remained between 40% and 50% over the time course of treatment. In contrast, the percentage of BrdU-positive cells in the CI-1033-treated tumours decreased to less than 20% by day 3.

Effect of CI-1033 on uptake of the hypoxia tracers, FAZA and F-MISO

Solid tumours are generally less well oxygenated than normal tissues, resulting in areas of hypoxia [46], particularly within central regions of the tumour. To determine the effect of CI-1033 treatment on tumour hypoxia, we employed the recently validated PET hypoxia tracer FAZA [35] (Fig. 3). Typical FAZA PET images for control and CI-1033-treated animals (Fig. 3a) revealed a degree of heterogeneity in tumour uptake in both controls and CI-1033-treated animals, particularly at baseline and day 3. This is in contrast to the heterogeneity observed in FLT uptake, which was much more prominent in tumours of control animals compared to those of CI-1033-treated animals. By day 6, however, FAZA uptake in the CI-1033-treated group had diminished considerably and appeared more homogeneous. This most likely reflects the nature of tumour hypoxia, which may be transient in any given region of a tumour depending on local blood supply. FAZA PET-derived tumour to background ratios for the total cohort of animals averaged 6.9 on day 0. Despite the heterogeneity, mean FAZA PET uptake ratios (Table 2) showed that in CI-1033-treated tumours FAZA uptake decreased at day 3 by approximately 50% (0.48±0.12) relative to baseline, with little further change at day 6 (0.43± 0.14). In the control tumours, FAZA uptake was stable between days 0 and 3 but increased slightly at day 6 (1.28± 0.09). Therefore, over the 6-day treatment period, FAZA uptake in CI-1033-treated tumours was reduced by approximately 66% compared to controls ($p>0.001$).

To compare FAZA as a hypoxia-imaging agent with the currently more widely employed agent, F-MISO, mice previously scanned with FAZA were subjected to a single F-MISO scan on day 7. Comparison of FAZA and F-MISO images for a typical control animal are shown in Fig. 3b. As can be seen, background signals are fairly similar for the two tracers, both showing a high level of signal for tracer clearance through the GI tract. Mean uptake ratios calculated from FAZA (day 6) and F-MISO (day 7) scans (Table 3) show similar uptake of the two tracers into tumours of CI-1033-treated animals. However, tumour uptake of both tracers was low in the drug-treated group by

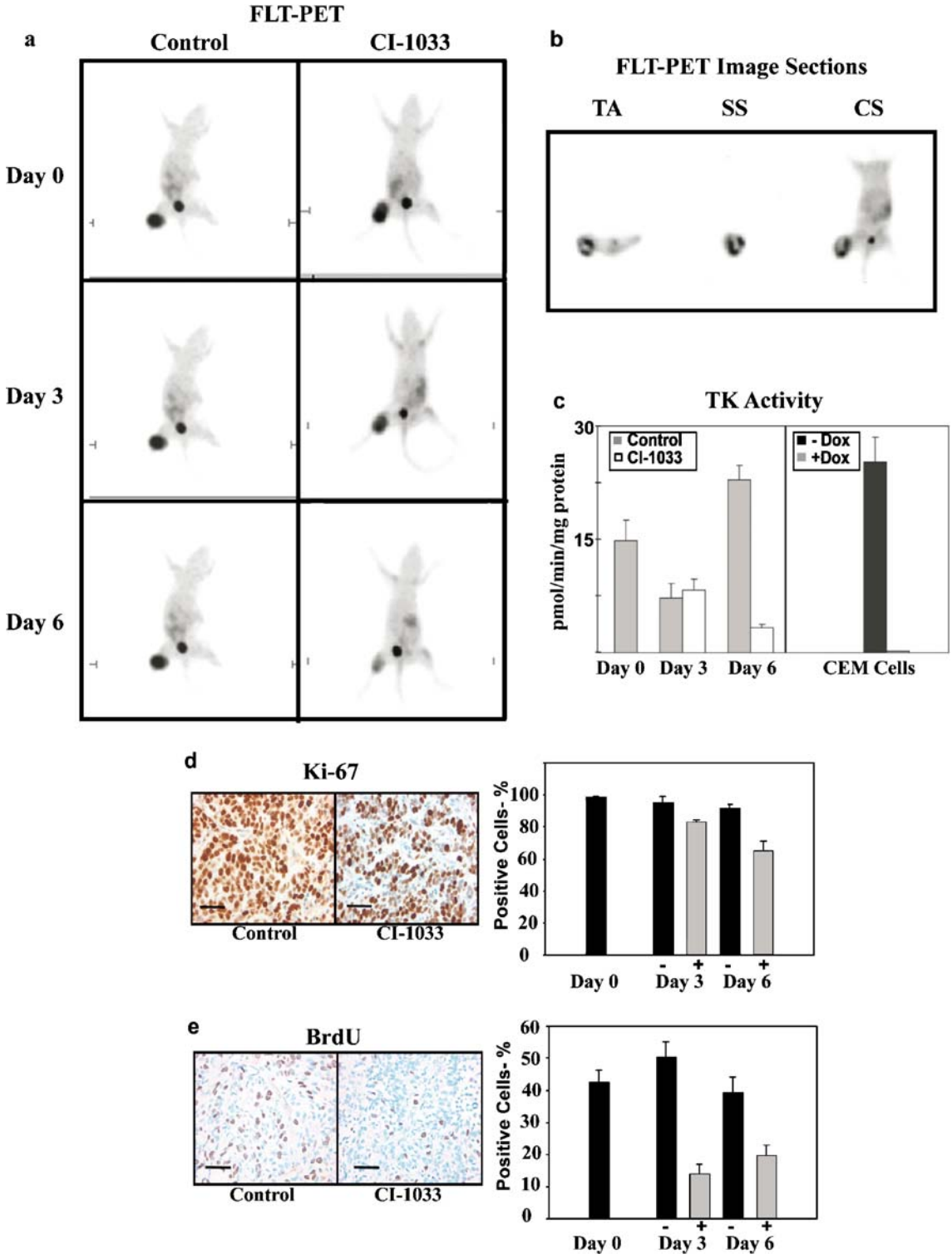

Fig. 2. FLT PET monitoring of CI-1033 treatment. **a** Examples of FLT PET images for typical control and CI-1033-treated animals on days 0, 3 and 6. Mice treated as described for Fig. 1 (*n*=7 control and 8 CI-1033) were scanned with FLT PET on days 0, 3 and 6. Image display as described for Fig. 1a **b** Example of heterogeneous FLT uptake in a control tumour at day 3. FLT image displayed as transaxial (*TA*), sagittal (*SS*) and coronal (*CS*) sections through the tumour region. **c** *Left panel*: TK activity was assayed in proteins extracted from control (*grey bars*) and CI-1033-treated (*white bars*) tumours at days 0, 3 and 6. *Right panel*: TK activity in proteins extracted from CEM cells expressing p16 from a tetracycline-inducible plasmid in the absence (*black bar*) or presence (*grey bar*) of doxycycline. Animals treated as described for Fig. 1c. **d, e** Anti-Ki-67 and anti-BrdU IHC, respectively. *Left*: Examples of tumour sections from control and CI-1033-treated mice (*n*=3 per group), as indicated, stained with antibodies to Ki-67 (day 3) or BrdU (day 6). *Right*: Mean±SD percentages of Ki-67- or BrdU-positive cells in control (*black bars*) and CI-1033-treated (*grey bars*) sections at days 0, 3 and 6. Treatment and tissue preparation are as in the legend to Fig. 1c except that mice were sacrificed 1 h after injection of 100 mg/kg BrdU

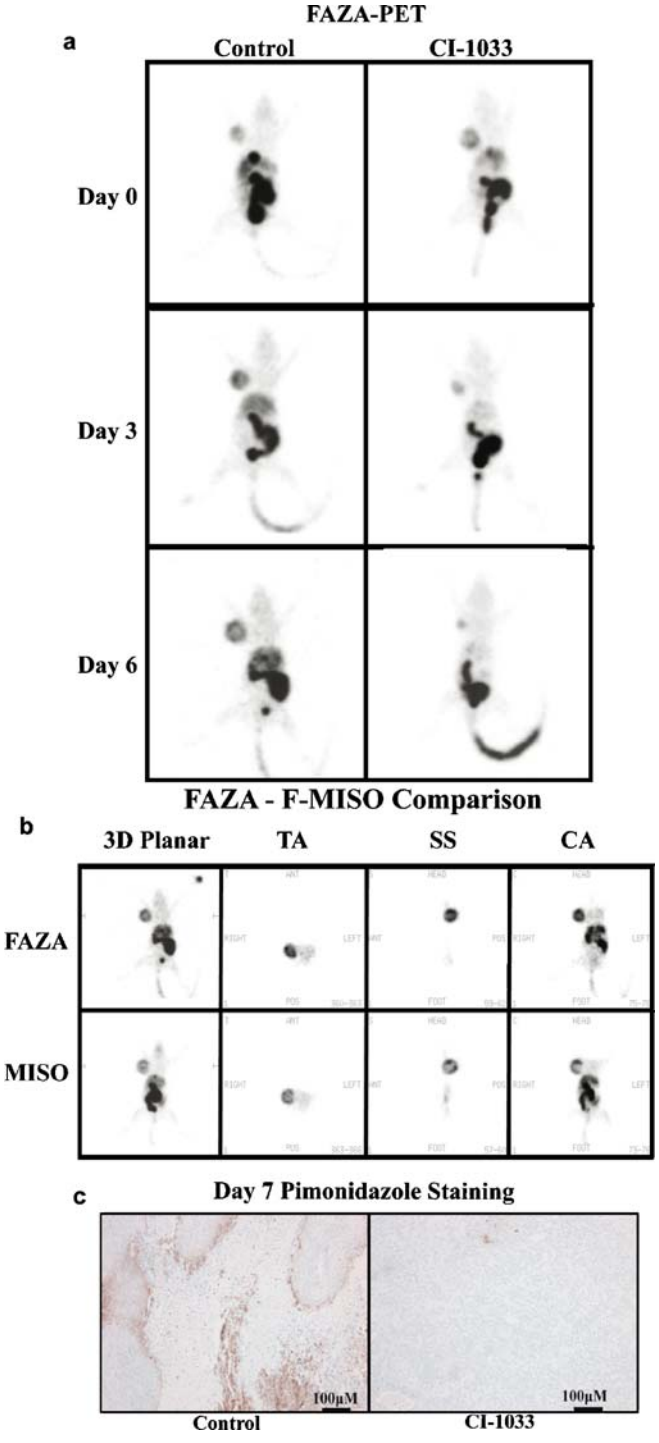

Fig. 3. FAZA/F-MISO PET monitoring of CI-1033 treatment. **a** Examples of FAZA PET images for typical control and CI-1033-treated animals. Mice treated as described for Fig. 1 (n=6) were scanned with FAZA PET on days 0, 3 and 6. Images displayed as described for Fig. 1a. **b** Typical PET images for a control animal. Mice scanned with FAZA on day 6 (*upper panels*) were re-scanned with F-MISO (*MISO*) on day 7 (*lower panels*). *Left to right*: 3D planar view, transaxial slice through tumour region (*TA*), sagittal section through tumour (*SS*) and coronal slice through the animal at the level of the tumour centre (*CA*). **c** Anti-pimonidazole IHC. Treatment and tissue preparation are as in the legend to Fig. 1 except that animals (n=2 per group) were sacrificed on day 7 at 3 h post injection of 60 mg/kg pimonidazole. Typical sections from control and CI-1033-treated tumours, as indicated, probed with anti-pimonidazole antibodies and photographed at 10× magnification

days 6 and 7, making comparison difficult. In the control animals, on the other hand, higher levels of hypoxia were observed on days 6 and 7 and in these animals the mean uptake ratio relative to day 0 was approximately 20% higher for FAZA than for F-MISO. This is despite the fact that tumour volumes in the control group increased by more than 15% between scan days 6 and 7 (mean volume day 6=2.49, day 7=2.92), which may have been expected to increase the degree of hypoxia on day 7. Examination of the raw data revealed that the lower uptake ratio for F-MISO was due to generally higher retention in mediastinal background regions compared to that of FAZA (data not shown).

For validation of the degree of hypoxia in the A431 tumours following 7 days of CI-1033 treatment, two animals each from control and treated groups were injected with pimonidazole, a nitroimidazole that, like FAZA, is retained in hypoxic cells [47]. Pimonidazole retention was visualised with anti-pimonidazole IHC on the sectioned tumours. As can be seen in Fig. 3c, there was a high level of pimonidazole staining in control tumour sections while staining was almost undetectable in CI-1033-treated tumours. As there were so few positively stained cells in the drug-treated sections, no quantification was performed; however, a large number of fields were examined and the images presented are typical of staining patterns for central regions of tumours from control and CI-1033-treated animals.

As tumours regressed in response to CI-1033 treatment, the extent of apoptosis in tumours of treated and control animals was assessed by IHC with anti-active caspase-3 antibodies. In this assay, very few cells in sections from either control or CI-1033-treated animals were positively stained (not shown). Scoring of these sections revealed that 1.8±0.5% of cells in baseline tumour sections were positive for active caspase-3. While the positive fraction increased by approximately 50% relative to baseline in the CI-1033-treated tumours (day 3=3.6±0.7%; day 6=3.3±0.9%), there was a similar increase in numbers of stained cells in control tumours (day 3=2.7±0.9%; 3.0±0.7%). The increase in positive cells in the control tumours was due mainly to the

Table 3. Uptake ratios for FAZA versus F-MISO[a]

Group[b]	FAZA	F-MISO
	Day 6	Day 7
Control	1.28±0.09	1.02±0.17
CI-1033	0.43±0.14	0.37±0.16

[a]Mean change in tumour to background ratio ±SEM, compared to baseline (day 0)
[b]n= 6

appearance of occasional clusters of positive cells in the larger control tumours at days 3 and 6 while in CI-1033-treated tumours, the few positive cells were dispersed throughout the tumour tissue. This analysis failed to reveal a significant level of caspase-3 activation within the 6 days of CI-1033 treatment, suggesting that the mechanism by which CI-1033 induces A431 tumour regression may not involve classical caspase activation pathways.

Discussion

The aim of this study was to evaluate small animal PET imaging to define changes in cellular metabolism, proliferation and hypoxia associated with the in vivo tumour response to molecularly targeted therapy. We chose the pan-EGFR/Erb-B inhibitor, CI-1033, as a representative of an important class of anti-cancer agents targeting cell surface receptor tyrosine kinase proto-oncogenes. As a tumour target we used the aggressively growing xenograft model, A431, which highly over-expresses EGFR and responds well to Erb-B-targeted drugs [48, 49]. Further, A431 tumours demonstrate excellent uptake of a range of PET tracers [41], making it an ideal model for a multi-tracer PET imaging investigation of functional changes in response to EGFR/Erb-B-targeted therapeutics.

Based on the FDG PET data, metabolic activity was reduced in tumours of CI-1033-treated animals and this finding was confirmed by ex vivo counting of retained FDG radioactivity on the final scanning day (Fig. 1b). High FDG uptake in many tumours compared to most normal tissues is thought to be a consequence of up-regulation of expression and/or activity of glucose transporters, particularly Glut1, and metabolic enzymes such as hexokinase [43, 50]. Both Glut1 expression and hexokinase activity are stimulated by activation of the EGFR/Erb-B pathway [51, 52]. Consistent with tumour-specific reduction in FDG uptake on PET, a striking reduction in Glut1 staining intensity was observed in CI-1033-treated tumour sections compared to controls. Together these data suggest that CI-1033-mediated down-regulation of EGFR/Erb-B signal transduction in A431 cells contributes to reduction in glycolytic metabolism, which may be a factor in the therapeutic outcome for anti-Erb-B targeted agents.

As glycolytic metabolism is important for maintenance of cell growth and division, changes in FDG uptake are likely to be accompanied by alterations in other cellular pathways, including those regulating proliferation. PET-derived uptake ratios revealed that by day 6 of treatment, tumours in CI-1033 mice retained only half as much FLT as control animals suggesting a potent anti-proliferative response. When FDG and FLT results are compared, relative uptake ratios for the two tracers follow similar trends on both imaging days. However, the average tumour to background ratio for the total cohort of FLT-imaged animals at baseline (n=15) was 8.4, compared to 5.4 for the FDG-imaged group (n=16). This is due to generally better FLT retention in tumour tissue, as well as slightly reduced background signal for FLT versus FDG. Therefore, FLT compares favourably with FDG as a viable clinical tool for monitoring anti-tumour therapy with PET.

In a recent report, FDG and FLT were compared for monitoring of the A431 response in mice treated with an Erb-B1 and 2 inhibitor, PKI-166 [53]. In that case, the mean pre-treatment tumour to background ratio was 0.83±0.04 for FDG and 9.5±1.0 for FLT (n=4). It is not clear why the FDG uptake ratio differs strikingly from the 5.4 observed in our study as the data sets were calculated from PET images using similar methodology. However, comparison of example images shown for the two studies suggests that the main difference may lie in a higher background signal for FDG in the Waldherr et al. report. Data presented herein were generated in fasted Balb/c *Nu/Nu* mice imaged for 5 min at 90 min post injection of 11–22 MBq FDG. Waldherr et al. reported data generated in SCID mice imaged for 15 min at 60 min post injection of 7.4 MBq FDG (feeding status not mentioned). It is therefore possible that differences in FDG tumour to background ratios in the two studies are attributable to either variation in rates of FDG clearance from normal tissues in the two mouse strains or technical procedures for animal preparation and imaging. Importantly, however, FLT uptake ratios are quite similar in the two studies, confirming the utility of FLT as a PET imaging agent for tumour monitoring. Furthermore, in both studies, significant reduction in FLT uptake into tumours was detected by PET following anti-Erb-B targeted therapy.

FLT retention within tumour cells is thought to be tightly correlated with cytosolic TK activity [54], which varies considerably during the cell cycle. TK activity peaks in S phase and is low in G1, due to both a tenfold reduction in synthesis rate and decreased protein stability following cell division [55]. Phosphorylation of TK also varies through the cell cycle [56], providing a further regulatory mechanism. In the present study, TK activity in CI-1033-treated tumours decreased to about 50% of baseline level at day 3, with a further decline to about 20% of baseline at day 6. These changes correlated with the observed reductions in PET-derived FLT uptake into tumours of CI-1033-treated animals. However, a reduction in TK activity was also observed in tumours of control animals at day 3 and the reason for this is not clear, as FLT uptake on PET had increased in the control tumours at day 3 (Table 2).

One possible explanation for the discrepancy between FLT uptake and TK activity in day 3 controls is that FLT uptake into larger tumours is often heterogeneous, varying considerably within different regions of the tumour mass. In many such cases, FLT uptake is high near the rim of the tumour but completely absent from pockets of cells within central regions (see Fig. 2b). In the TK assay, activity is calculated relative to weight of tumour protein assayed, while PET derived tumour to background ratio is independent of tumour volume. Therefore, areas transiently lacking TK activity may have served to reduce ex vivo TK activity without affecting FLT uptake in control tumours at day 3. Further, it has been shown that TK activity is dependent on several factors, including protein expression level and the presence of co-factors for catalysis [57]. It is possible that

the influence of these factors may vary between in vivo and ex vivo situations. Therefore, it is possible that while TK activity is the major influence on FLT uptake, other factors may play a role in tumour retention of FLT in vivo.

At day 6 of the study, TK activity in tumours of the control group had increased to approximately 150% of baseline while in CI-1033 tumours there was a considerable reduction in activity. Therefore, by the end of the treatment period TK levels in tumours of control animals were about sevenfold higher than in the CI-1033-treated group, in agreement with significantly stronger FLT uptake in control versus CI-1033-treated tumours in the day 6 scans. Consistent with TK activity and FLT PET data, numbers of cells incorporating BrdU at day 6 had dropped by about 50% in the CI-1033 tumours compared to controls. Ki-67 levels in the CI-1033-treated tumours also declined; however, approximately 75% of cells still expressed Ki-67 at day 6. Ki-67 is expressed in all cell cycle phases except G_0 [58] while BrdU incorporation occurs during mitosis. Taken together, data from Ki-67 and BrdU IHC suggest that cells in CI-1033-treated tumours are not actively cycling but have not exited into G_0. This is consistent with previously reported findings that CI-1033 treatment causes G_1 arrest in colonic tumour cell lines in culture [33].

Anti-caspase 3 immunoblots of the CI-1033-treated tumours did not indicate increased levels of apoptosis compared to controls during a 6-day treatment period. This may seem surprising in light of the significant volume reduction of CI-1033-treated tumours. However, previous studies have reported varying levels of apoptosis in different cell lines responding to CI-1033. For instance, CI-1033 treatment elicited a significant level of apoptosis in Caco-2 cells but virtually none in LoVo cells, although EGFR phosphorylation and cellular growth were blocked in both colonic tumour cell lines [33]. In an earlier study, Nelson and Fry [59] also found dramatically different levels of apoptosis upon exposure of MDA-MB-231 and MCF7 breast tumour cell lines to CI-1033. Therefore, it is possible that the A431 response to CI-1033 may involve caspase-independent cell death pathways such as mitotic catastrophe or necrosis [60]. In relation to the latter, however, in histological examination there was no evidence of large areas of necrosis in the CI-1033-treated tumours. It is also possible that volume changes in the CI-1033-treated tumours are due to effects on other systems such as blood flow or fluid balance, rather than immediate cell death.

Signal transduction pathways that sense and respond to reduced oxygen tension have been associated with regulation of both cell cycle progression and glycolytic metabolism [12, 61]. Therefore, monitoring tumour hypoxia can yield important information regarding the nature of the response to molecularly targeted therapy. Results of both FAZA PET imaging and pimonidazole retention assays revealed that CI-1033 treatment significantly affects A431 tumour hypoxia. This may be partially attributed to reduced volume in the CI-0133-treated tumours, rendering central regions more accessible to blood flow and oxygen exchange. Concomitantly, increased volume of control tumours could serve to reduce oxygen access and increase hypoxia. In a previous study conducted by members of our team with other colleagues [62], treatment of A431 tumour-bearing mice with Gefitinib, a specific inhibitor of EGFR kinase activity, was shown to reduce tumour uptake of FAZA independently of changes in tumour volume. Because CI-1033 has a more immediate affect on tumour volume than Gefitinib (at the doses used for the two studies), it was not possible in the present study to rule out some volume effect. However, data from the Gefitinib/FAZA imaging study clearly support the notion that inhibition of EGFR/Erb-B activity affects A431 tumour oxygenation through means other than volume changes alone.

A further mechanism that may play a role in the observed CI-1033 hypoxia effect is blockade of EGFR/Erb-B signalling in endothelial cells contributing to normalisation of tumour vasculature. It has been shown that vascular endothelial cells express Erb-B receptors [63] and that activation of these cells with the Erb-B 3/4 ligand, heregulin, elicits an angiogenic response. Furthermore, Petit et al. [64] reported that injection of anti-EGFR neutralising antibody into A431 tumour xenografts suppresses vascular endothelial growth factor (VEGF) expression and causes a significant reduction in tumour blood vessel count. These workers suggested that effectiveness of anti-Erb-B receptor therapy may in part be due to anti-angiogenic effects that serve to increase therapeutic index over that expected from cytostatic effects alone. It will therefore be of future interest to examine the effect of CI-1033 on the expression of molecules that are directly related to tumour vascularity such as VEGF or its receptor.

In conclusion, we have shown that response to therapeutic targeting of EGFR/Erb-B kinase activity in A431 tumour xenografts can be readily assessed by PET using tracers for metabolism, proliferation and hypoxia. This conclusion is supported by results of ex vivo analyses of biomarkers for related tumour-associated processes. The results highlight the interrelatedness of signalling pathways regulating important aspects of tumour growth and show that a single targeted therapeutic can have multiple functional outcomes in tumour cells. Further, the data presented indicate the power of PET for describing phenotypic changes in tumours during treatment and reinforce the notion that pre-clinical PET can make important contributions to the development of molecularly targeted anti-cancer therapeutics.

Acknowledgements. The Pre-clinical Imaging Facility was established at the Peter MacCallum Cancer Centre with a grant from the Pfizer Corporation (formerly Pharmacia) and all experimental work was supported by Pfizer Global Clinical Platforms Division. The authors acknowledge expert technical assistance provided by Ms. Susan Jackson. All experiments complied with current laws of Australia including ethics approval.

References

1. Tibes R, Trent J, Kurzrock R. Tyrosine kinase inhibitors and the dawn of molecular cancer therapeutics. Annu Rev Pharmacol Toxicol 2005;45:357–384
2. Sawyers C. Targeted cancer therapy. Nature 2004;432:294–297
3. Solomon B, McArthur G, Cullinane C, Zalcberg J, Hicks R. Applications of positron emission tomography in the development of molecular targeted cancer therapeutics. BioDrugs 2003; 17:339–354
4. Kelloff GJ, Hoffman JM, Johnson B, Scher HI, Siegel BA, Cheng EY, et al. Progress and promise of FDG-PET imaging for cancer patient management and oncologic drug development. Clin Cancer Res 2005;11:2785–2808
5. Scanga DR, Martin WH, Delbeke D. Value of FDG PET imaging in the management of patients with thyroid, neuroendocrine, and neural crest tumors. Clin Nucl Med 2004;29:86–90
6. Avril NE, Weber WA. Monitoring response to treatment in patients utilizing PET. Radiol Clin North Am 2005;43:189–204
7. Lyons SK. Advances in imaging mouse tumour models in vivo. J Pathol 2005;205:194–205
8. Herschman HR. Micro-PET imaging and small animal models of disease. Curr Opin Immunol 2003;15:378–384
9. Roselt P, Meikle S, Kassiou M. The role of positron emission tomography in the discovery and development of new drugs; as studied in laboratory animals. Eur J Drug Metab Pharmacokinet 2004;29:1–6
10. Maschauer S, Prante O, Hoffmann M, Deichen JT, Kuwert T. Characterization of ^{18}F-FDG uptake in human endothelial cells in vitro. J Nucl Med 2004;45:455–460
11. Rajendran JG, Wilson DC, Conrad EU, Peterson LM, Bruckner JD, Rasey JS, et al. [^{18}F]FMISO and [^{18}F]FDG PET imaging in soft tissue sarcomas: correlation of hypoxia, metabolism and VEGF expression. Eur J Nucl Med Mol Imaging 2003;30:695–704
12. Plas DR, Thompson CB. Cell metabolism in the regulation of programmed cell death. Trends Endocrinol Metab 2002;13:75–78
13. Elstrom RL, Bauer DE, Buzzai M, Karnauskas R, Harris MH, Plas DR, et al. Akt stimulates aerobic glycolysis in cancer cells. Cancer Res 2004;64:3892–3899
14. Vesselle H, Grierson J, Muzi M, Pugsley JM, Schmidt RA, Rabinowitz P, et al. In vivo validation of 3'deoxy-3'-[^{18}F] fluorothymidine ([^{18}F]FLT) as a proliferation imaging tracer in humans: correlation of [^{18}F]FLT uptake by positron emission tomography with Ki-67 immunohistochemistry and flow cytometry in human lung tumors. Clin Cancer Res 2002;8:3315–3323
15. Shields AF, Grierson JR, Dohmen BM, Machulla HJ, Stayanoff JC, Lawhorn-Crews JM, et al. Imaging proliferation in vivo with [F-18]FLT and positron emission tomography. Nat Med 1998;4:1334–1336
16. Piert M, Machulla H-J, Picchio M, Reischl G, Ziegler S, Kumar P, et al. Hypoxia-specific tumor imaging with ^{18}F-fluoroazomycin arabinoside. J Nucl Med 2005;46:106–113
17. Sorger D, Patt M, Kumar P, Wiebe LI, Barthel H, Seese A, et al. [^{18}F]fluoroazomycinarabinofuranoside (^{18}FAZA) and [^{18}F] fluoromisonidazole (^{18}FMISO): a comparative study of their selective uptake in hypoxic cells and PET imaging in experimental rat tumors. Nucl Med Biol 2003;30:317–326
18. Grierson JR, Schwartz JL, Muzi M, Jordan R, Krohn KA. Metabolism of 3'-deoxy-3'-[F-18]fluorothymidine in proliferating A549 cells: validations for positron emission tomography. Nucl Med Biol 2004;31:829–837
19. Barthel H, Cleij MC, Collingridge DR, Hutchinson OC, Osman S, He Q, et al. 3'-deoxy-3'-[^{18}F]fluorothymidine as a new marker for monitoring tumor response to antiproliferative therapy in vivo with positron emission tomography. Cancer Res 2003;63:3791–3798
20. Bradshaw HD Jr. Molecular cloning and cell cycle-specific regulation of a functional human thymidine kinase gene. Proc Natl Acad Sci U S A 1983;80:5588–5591
21. Sherley JL, Kelly TJ. Regulation of human thymidine kinase during the cell cycle. J Biol Chem 1988;263:8350–8358
22. Nunn A, Linder K, Strauss HW. Nitroimidazoles and imaging hypoxia. Eur J Nucl Med 1995;22:265–280
23. Hockel M, Vaupel P. Tumor hypoxia: definitions and current clinical, biologic, and molecular aspects. J Natl Cancer Inst 2001;93:266–276
24. Baselga J, Arteaga CL. Critical update and emerging trends in epidermal growth factor receptor targeting in cancer. J Clin Oncol 2005;23:2445–2459
25. Abd El-Rehim DM, Pinder SE, Paish CE, Bell JA, Rampaul RS, Blamey RW et al. Expression and co-expression of the members of the epidermal growth factor receptor (EGFR) family in invasive breast carcinoma. Br J Cancer 2004;91:1532–1542
26. Ioachim E, Kamina S, Athanassiadou S, Agnantis NJ. The prognostic significance of epidermal growth factor receptor (EGFR), C-erbB-2, Ki-67 and PCNA expression in breast cancer. Anticancer Res 1996;16(5B):3141–3147
27. Tsuda H, Morita D, Kimura M, Shinto E, Ohtsuka Y, Matsubara O et al. Correlation of KIT and EGFR overexpression with invasive ductal breast carcinoma of the solid-tubular subtype, nuclear grade 3, and mesenchymal or myoepithelial differentiation. Cancer Sci 2005;96:48–53
28. Hynes NE, Lane HA. ERBB receptors and cancer: the complexity of targeted inhibitors. Nat Rev Cancer 2005;5:341–354
29. Allen LF, Lenehan PF, Eiseman IA, Elliott WL, Fry DW. Potential benefits of the irreversible pan-erbB inhibitor, CI-1033, in the treatment of breast cancer. Semin Oncol 2002;29:11–21
30. Slichenmyer WJ, Elliott WL, Fry DW. CI-1033, a pan-erbB tyrosine kinase inhibitor. Semin Oncol 2001;28:80–85
31. Smaill JB, Rewcastle GW, Loo JA, Greis KD, Chan OH, Reyner EL, et al. Tyrosine kinase inhibitors. 17. Irreversible inhibitors of the epidermal growth factor receptor: 4-(phenylamino)quinazoline- and 4-(phenylamino)pyrido[3,2-d]pyrimidine-6-acrylamides bearing additional solubilizing functions. J Med Chem 2000;43:1380–1397
32. Erlichman C, Boerner SA, Hallgren CG, Spieker R, Wang X-Y, James CD, et al. The HER tyrosine kinase inhibitor CI1033 enhances cytotoxicity of 7-ethyl-10-hydroxycamptothecin and topotecan by inhibiting breast cancer resistance protein-mediated drug efflux. Cancer Res 2001;61:739–748
33. Nyati MK, Maheshwari D, Hanasoge S, Sreekumar A, Rynkiewicz SD, Chinnaiyan AM, et al. Radiosensitization by pan ErbB inhibitor CI-1033 in vitro and in vivo. Clin Cancer Res 2004;10:691–700
34. Machulla HJ, Blocher A, Kuntzsch M, Piert M, Wei R, Grierson JR. Simplified labeling approach for synthesizing 3'-deoxy-3'-[^{18}F]fluorothymidine ([^{18}F]FET). J Radioanal Nucl Chem 2000;243:843–846
35. Piert M, Machulla HJ, Kumar P, Link T, Wiebe LI. ^{18}F labeled fluoroazamycin arabinoside (FAZA): a novel marker of tumour tissue hypoxia. J Nucl Med 2001;42:279
36. Surti S, Karp JS, Perkins AE, Freifelder R. TNSG. M. Design evaluation of A-PET: A high sensitivity animal PET camera. Trans Nucl Sci 2003;50:1357–1363

37. Chiang S, Cardi C, Matej S, Zhuang H, Newberg A, Alavi A, et al. Clinical validation of fully 3-D versus 2.5-D RAMLA reconstruction on the Philips-ADAC CPET PET scanner. Nucl Med Commun 2004;25:1103–1107
38. Tanaka E, Kudo H. Subset-dependent relaxation in block-iterative algorithms for image reconstruction in emission tomography. Phys Med Biol 2003;48:1405–1422
39. Deans AJ, Simpson KJ, Trivett MK, Brown MA, McArthur GA. Brca1 inactivation induces p27(Kip1)-dependent cell cycle arrest and delayed development in the mouse mammary gland. Oncogene 2004;23:6136–6145
40. Stuart P, Ito M, Stewart C, Conrad SE. Induction of cellular thymidine kinase occurs at the mRNA level. Mol Cell Biol 1985;5:1490–1497
41. Solomon B, Hagekyriakou J, Trivett MK, Stacker SA, McArthur GA, Cullinane C. EGFR blockade with ZD1839 ("Iressa") potentiates the antitumor effects of single and multiple fractions of ionizing radiation in human A431 squamous cell carcinoma. Epidermal growth factor receptor. Int J Radiat Oncol Biol Phys 2003;55:713–723
42. Sirotnak FM, Zakowski MF, Miller VA, Scher HI, Kris MG. Efficacy of cytotoxic agents against human tumor xenografts is markedly enhanced by coadministration of ZD1839 (Iressa), an inhibitor of EGFR tyrosine kinase. Clin Cancer Res 2000;6:4885–4892
43. Avril N. GLUT1 expression in tissue and ^{18}F-FDG uptake. J Nucl Med 2004;45:930–932
44. Mueckler M. Facilitative glucose transporters. Eur J Biochem 1994;219:713–725
45. Toyohara J, Waki A, Takamatsu S, Yonekura Y, Magata Y, Fujibayashi Y. Basis of FLT as a cell proliferation marker: comparative uptake studies with [^{3}H]thymidine and [^{3}H] arabinothymidine, and cell-analysis in 22 asynchronously growing tumor cell lines. Nucl Med Biol 2002;29:281–287
46. Guppy M. The hypoxic core: a possible answer to the cancer paradox. Biochem Biophys Res Commun 2002;299:676–680
47. Overgaard J. Clinical evaluation of nitroimidazoles as modifiers of hypoxia in solid tumors. Oncol Res 1994;6:509–518
48. Anderson NG, Ahmad T, Chan K, Dobson R, Bundred NJ. ZD1839 (Iressa), a novel epidermal growth factor receptor (EGFR) tyrosine kinase inhibitor, potently inhibits the growth of EGFR-positive cancer cell lines with or without erbB2 overexpression. Int J Cancer 2001;94:774–782
49. Matar P, Rojo F, Cassia R, Moreno-Bueno G, Di Cosimo S, Tabernero J, et al. Combined epidermal growth factor receptor targeting with the tyrosine kinase inhibitor gefitinib (ZD1839) and the monoclonal antibody cetuximab (IMC-C225): superiority over single-agent receptor targeting. Clin Cancer Res 2004;10:6487–6501
50. Macheda ML, Rogers S, Best JD. Molecular and cellular regulation of glucose transporter (GLUT) proteins in cancer. J Cell Physiol 2005;202:654–662
51. Mischoulon D, Rana B, Kotliar N, Pilch PF, Bucher NL, Farmer SR. Differential regulation of glucose transporter 1 and 2 mRNA expression by epidermal growth factor and transforming growth factor-beta in rat hepatocytes. J Cell Physiol 1992;153:288–296
52. Bryson JM, Coy PE, Gottlob K, Hay N, Robey RB. Increased hexokinase activity, of either ectopic or endogenous origin, protects renal epithelial cells against acute oxidant-induced cell death. J Biol Chem 2002;277:11392–11400
53. Waldherr C, Mellinghoff IK, Tran C, Halpern BS, Rozengurt N, Safaei A, et al. Monitoring antiproliferative responses to kinase inhibitor therapy in mice with 3'-deoxy-3'-18 F-fluorothymidine PET. J Nucl Med 2005;46:114–120
54. Rasey JS, Grierson JR, Wiens LW, Kolb PD, Schwartz JL. Validation of FLT uptake as a measure of thymidine kinase-1 activity in A549 carcinoma cells. J Nucl Med 2002;43:1210–1217
55. Sherley JL, Kelly TJ. Regulation of human thymidine kinase during the cell cycle. J Biol Chem 1988;263:8350–8358
56. Lin L, Kuroiwa N, Moriyama Y, Fujimura S. Continuous increase in phosphorylation of cytosolic thymidine kinase during proliferation of rat hepatoma JB1 cells. Oncol Rep 2003;10:665–669
57. Barthel H, Cleij MC, Collingridge DR, Hutchinson OC, Osman S, He Q, et al. 3'-deoxy-3'-[^{18}F]fluorothymidine as a new marker for monitoring tumor response to antiproliferative therapy in vivo with positron emission tomography. Cancer Res 2003;63:3791–3798
58. Gerdes J, Becker MH, Key G, Cattoretti G. Immunohistological detection of tumour growth fraction (Ki-67 antigen) in formalin-fixed and routinely processed tissues. J Pathol 1992;168:85–86
59. Nelson JM, Fry DW. Akt, MAPK (Erk1/2), and p38 act in concert to promote apoptosis in response to ErbB receptor family inhibition. J Biol Chem 2001;276:14842–14847
60. Broker LE, Kruyt FA, Giaccone G. Cell death independent of caspases: a review. Clin Cancer Res 2005;11:3155–3162
61. Robey IF, Lien AD, Welsh SJ, Baggett BK, Gillies RJ. Hypoxia-inducible factor-1alpha and the glycolytic phenotype in tumors. Neoplasia 2005;7:324–330
62. Solomon B, Binns D, Roselt P, Weibe LI, McArthur GA, Cullinane C, et al. Modulation of intratumoral hypoxia by the epidermal growth factor receptor inhibitor gefitinib detected using small animal PET imaging. Mol Cancer Ther 2005;4:1417–1422
63. Russell KS, Stern DF, Polverini PJ, Bender JR. Neuregulin activation of ErbB receptors in vascular endothelium leads to angiogenesis. Am J Physiol 1999;277:H2205–H2211
64. Petit AM, Rak J, Hung MC, Rockwell P, Goldstein N, Fendly B, et al. Neutralizing antibodies against epidermal growth factor and ErbB-2/neu receptor tyrosine kinases down-regulate vascular endothelial growth factor production by tumor cells in vitro and in vivo: angiogenic implications for signal transduction therapy of solid tumors. Am J Pathol 1997;151:1523–1530